Materials Research. 2022; 25:e20220012
DOI: https://doi.org/10.1590/1980-5373-MR-2022-0012

Green Eugenol Oligomers as Corrosion Inhibitors for Carbon Steel in 1M HCl

Luana B. Furtado[a]*, Rafaela C. Nascimento[b], Maria José O. C. Guimarães[a], Simone L. D. C. Brasil[c], Sergio H. R. Barra[a]

[a]*Universidade Federal do Rio de Janeiro, Escola de Química, Departamento de Processos Orgânicos, Rio de Janeiro, RJ, Brasil.*
[b]*Universidade de Évora, Instituto de Investigação e Formação Avançada, LAQV-REQUIMTE, Colégio Luís António Verney, 7000-671 Évora, Portugal.*
[c]*Universidade Federal do Rio de Janeiro, Escola de Química, Departamento de Processos Inorgânicos, Rio de Janeiro, RJ, Brasil.*

Received: January 11, 2022; Revised: March 18, 2022; Accepted: April 27, 2022

This study investigated the corrosion inhibition of polyeugenol on API P110 in 1 M HCl. Its monomer – eugenol – is obtained from clove and cinnamon, making the oligomer environmentally friendly. The influence of molecular weight and polymerization degree was evaluated by increasing the polymerization initiator/monomer ratio. This enabled the polymerization of three different oligomers (P10, P20 and P30), which were characterized by Fourier-transform infrared spectroscopy (FTIR), proton nuclear magnetic resonance (^{1}H-NMR), thermogravimetric analysis (TGA/DTG), and size exclusion chromatography techniques. The inhibition performance of polyeugenol was determined by weight loss (WL) and electrochemical tests to assess the influence of structural differences. WL indicated that the oligomer with the lowest polymerization degree (P10) exhibited greater efficiency (82-84%) due to more uniform surface coverage. Electrochemical tests confirmed polyeugenol as a mixed inhibitor. Energy-dispersive X-ray spectroscopy (EDX) calculations indicated the presence of an organic layer covering the steel surface.

Keywords: *Polymeric inhibitor, Weight loss, Green corrosion inhibitor, Electrochemical measurements.*

1. Introduction

Corrosive processes affect the agricultural, civil construction, and oil and gas industries. In the oil and gas sector, carbon steel is widely used in transport pipelines, structures, and equipment. Since this material is subjected to corrosion, especially in acidic media, inhibitors are needed[1-4].

The development of corrosion inhibitors focuses on certain structural characteristics of molecules that favor adsorption on the metallic surface. Desirable structures include heteroatoms (N, P, O and S), lone pairs of electrons, unsaturation and aromatic rings[5-8]. Conventional inhibitors (azoles and chrome-based) cause environmental and health problems[9,10] and as a result, green corrosion inhibitors have garnered greater attention in recent years. These inhibitors should be easily available, low cost and exhibit high inhibition efficiency[11,12]. Green corrosion inhibitors have been developed from a variety of sources, including leaves[11,13-15], seeds[16-20], fruits[21], flowers[22], peel[23-25] and residual biomass[26].

Eugenol (4-allyl-2-methoxyphenol) is found in this eco-friendly context as the main component of clove leaves (74 wt.%), buds (50 wt.%) and cinnamon leaves (87.3 wt.%)[27-29]. This compound exhibits important antioxidant[30], antibiotic[31] and anti-inflammatory properties[32], and has been successfully used as a corrosion inhibitor for steel in acidic media[27]. Besides, the cationic polymerization of eugenol has been studied due to the presence of an allyl group in the structure[33-37]. However, polyeugenol has yet to be used in the field of corrosion.

In the present study, three novel oligomers obtained from eugenol were synthesized by varying the initiator/monomer ratio, and investigated as corrosion inhibitors for carbon steel in 1 M HCl. The oligomers were characterized by Fourier-transform infrared spectroscopy (FTIR), proton nuclear magnetic resonance (^{1}H-NMR), thermogravimetric analysis (TGA/DTG), and size exclusion chromatography (SEC). Weight loss measurements, linear polarization resistance (LPR) and potentiodynamic polarization (PDP) were performed to evaluate corrosion inhibition efficiency. Steel surface morphology was analyzed by scanning electron microscopy with energy-dispersive X-ray spectroscopy (SEM-EDX) and contact angle measurement.

2. Experimental

2.1. Oligomer synthesis

The methodology used was adapted from the literature[33] and is shown in Figure 1. The chemicals were obtained from Sigma-Aldrich. Eugenol (30.00 g) was added to a round-bottom flask under inert atmosphere (N_2). The initiator ($BF_3.OEt_2$) was first added at room temperature using the

*e-mail: luana_bf18@eq.ufrj.br

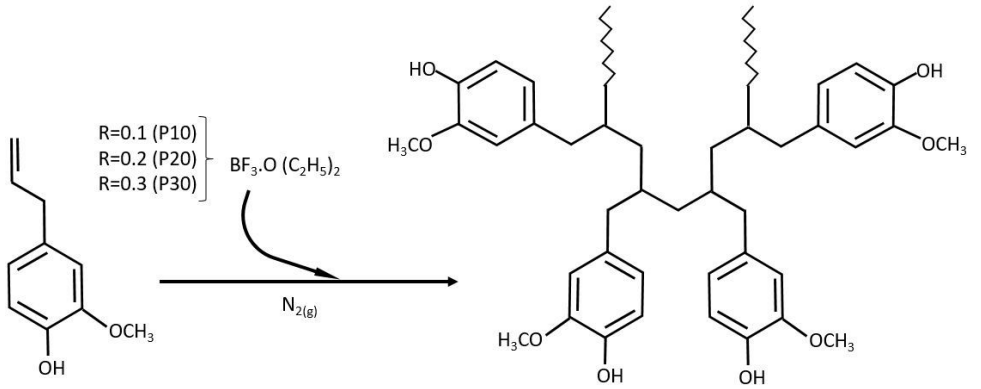

Figure 1. Synthetic route of eugenol oligomers using boron trifluoride etherate ($BF_3.OEt_2$) as initiator (R = g initiator/g eugenol).

following monomer-initiator ratios (Ri/m): 0.05, 0.10 and 0.15 g-initiator/g-eugenol. The solution color changed from pale yellow into dark red/violet. Next, the same mass of initiator was added after one hour, totaling 0.10, 0.20 and 0.30 g-initiator/g-eugenol. The reactions proceeded overnight, after which methanol (0.17 mL/g-eugenol) was added to each flask to stop polymerization. The products obtained (P10, P20 and P30) were then solubilized in chloroform (0.67 mL/g-eugenol).

2.2. Characterization

2.2.1. Fourier-transform infrared spectroscopy (FTIR)

The oligomers (P10, P20 and P30) were analyzed using a NICOLET 6700 Fourier Transform Infrared Spectrometer at 293 K. A total of 20 scans were performed from 4000 to 400 cm^{-1}, with a resolution of 4.00 cm^{-1}.

2.2.2. Proton nuclear magnetic resonance (^{1}H- NMR)

The oligomers (P10, P20 and P30) and eugenol were analyzed by ^{1}H-NMR in a Varian Mercury VX 300 spectrometer. The sample (10-15 mg) was solubilized in 0.8 mL of deuterated chloroform (CIL 99.8% d) and analyzed at 313 K, with a total of 20 scans and 20 s between pulses (delay-d1), at an observation frequency of 299.99 MHz.

2.2.3. Thermogravimetric analysis (TGA/DTG)

The thermal stability of the oligomers was monitored by thermogravimetric analysis (TGA) and differential thermogravimetric analysis (DTG) on a PerkinElmer equipment model Pyris 1 TGA/DSC. The sample (10 mg) was weighed in a ceramic pan and subjected to a temperature range of 298 to 998 K, with a heating rate of 10 K/min, under a N_2 flow of 30 mL/min.

2.2.4. Size exclusion chromatography (SEC)

Size exclusion chromatography was performed in a Prominence® UFLC Shimadzu chromatograph. Chloroform was used as eluent, at a rate of 1.0 mL/min, in two columns: Shin-pack SEC-803C (300 x 8.0 mm) and Phenogel™ 5 µm Linear (2) (300 x 7.8 mm), with exclusion limits of $7x10^4$ and $1x10^7$, respectively. The stationary phase in the columns consisted of spherical porous particles of styrene-divinylbenzene copolymers. After the samples were properly prepared for analysis, the analysis conditions were adjusted, being the temperature of 313 K in the columns and detectors, and flow of 1.0 mL/min. Monodisperse polystyrene standards were used for relative calibration. Finally, the 0.1% concentration sample was injected and the data processed, allowing the obtaining of the parameters M_w, M_n and polydispersion.

2.3. Weight loss measurements

Coupons (10 mm x 20 mm x 5 mm, 3 mm central hole) were obtained from a carbon steel sample (API P110), with the following composition (wt. %): C, 0.280; Mn, 1.220; Si, 0.280; P, 0.016; S, 0.002; Ni, 0.010; Mo, 0.110; and Fe, 98.1. The specimens were prepared before and after immersion according to ASTM G31[38]. The 24-h tests were performed in duplicate. The effect of concentration (0.5, 2.0, 3.5 and 5.0% v/v) was studied at 333 K and corrosion rates were calculated according to ASTM G31[38], as shown in Equation 1.

$$CR = \frac{K * \Delta m(g)}{A(cm^2) * \rho\left(\frac{g}{cm^3}\right) * t(h)} \quad (1)$$

where K is a constant, Δm weight loss, A the surface area of the sample, ρ sample density and t immersion time. Inhibition efficiency (IE_{WL}) was calculated according to Equation 2, where CR_0 and CR_{inh} are the corrosion rates in the absence and presence of the inhibitor, respectively.

$$IE_{WL}(\%) = \left(\frac{CR_0 - CR_{inh}}{CR_0}\right) * 100 \quad (2)$$

2.4. Electrochemical tests

Electrochemical tests were performed at room temperature, in a computer-controlled Autolab Potentiostat/Galvanostat (PGSTAT302N), using NOVA 2.1 software for linear polarization resistance (LPR) and potentiodynamic polarization (PDP). A three-electrode cell was used, with the carbon steel sample (working electrode), a

large-area platinum wire (counter electrode) and an Ag/AgCl electrode (reference electrode). A salt bridge (KCl saturated) was used to isolate the Ag/AgCl electrode from the test solution, preserving the reference electrode. Before polarization, the open-circuit potential (OCP) was monitored for 50 min until it reached a steady-state. The cathodic and anodic polarization curves were obtained separately in duplicate, within a range of 250 mV around E_{corr} ($E = E_{corr} \pm 250$ mV), at a scan rate of 0.333 mV s^{-1}. The LPR curves were obtained in quadruplicate, at a scan rate of 0.333 mV s^{-1} and within a range of 15 mV around E_{corr} ($E = E_{corr} \pm 15$ mV). This very low scan rate is typically applied and widely reported in the literature, and was adopted in order to clearly observe the reaction stages[39,40]. The inhibiting efficiencies obtained from PDP and LPR were calculated according to Equations 3 and 4, respectively.

$$IE_{PDP}(\%) = \left(\frac{I_{corr0} - I_{corrinh}}{I_{corr0}} \right) * 100 \quad (3)$$

$$IE_{LPR}(\%) = \left(\frac{R_{inh} - R_0}{R_{inh}} \right) * 100 \quad (4)$$

where parameter R is polarization resistance, and I_{corr} corrosion current density. The subscripts "inh" and "0" refer to the presence and absence of the inhibitor, respectively.

2.5. Scanning electron microscopy with energy-dispersive X-ray spectroscopy (SEM-EDX)

The API P110 carbon steel coupons submitted to 24-h immersion testing in 1 M HCl at 333 K, in the presence and absence of the corrosion inhibitor (P10) at 3.5% v/v, were analyzed by SEM-EDX using a Hitachi TM 3030 Plus instrument.

2.6. Contact angle

The contact angle of 2.5 µL water droplets on API P110 samples after corrosion tests with and without inhibitor (P10, 3.5% v/v) were analyzed by a Ossila Limited Contact Angle Goniometer (L2004A1). The measurements were made in duplicates, where the standard deviation was calculated.

3. Results and Discussion

3.1. Oligomer characterization

3.1.1. Fourier-transform infrared spectroscopy (FTIR)

The infrared spectra of eugenol and the oligomers (P10, P20 and P30) are shown in Figure 2. In Figure 2a-d, aromatic hydrogen stretching is related to the band at 1514 cm^{-1} (region 1), while the bands around 2850 cm^{-1} are associated with C_{sp3}-H stretching of aromatic rings[41,42]. Bands attributed to in-plane C-H aromatic angular deformation (1050-1100 cm^{-1})[43], and out-of-plane aromatic C-H angular deformation (720-880 cm^{-1})[44] are also present. The bands at 1268-1272 cm^{-1} (region 2) and 991-996 cm^{-1} (region 3) confirm the presence of vinylic hydrogen. Eugenol polymerization is validated by the decline in band intensity around 995 cm^{-1}, related to allyl groups of the monomer[33]. In Figure 2b-d, the intensity of these bands decreases as the initiator/monomer ratio ($R_{i/m}$) rises, confirming oligomer synthesis and improved reaction conversion.

3.1.2. Proton nuclear magnetic resonance (^{1}H-NMR)

Structural analyses of eugenol and its oligomers (P10, P20 and P30) by ^{1}H-NMR are observed in Figure 3. The chemical shifts at 0.90-1.57 ppm represent methyl hydrogen and the peaks at 2.61-2.88 ppm the –CH– hydrogen present in P10, P20 and P30, but absent in eugenol[45]. Both the methyl and –CH– signals increased with the initiator/monomer

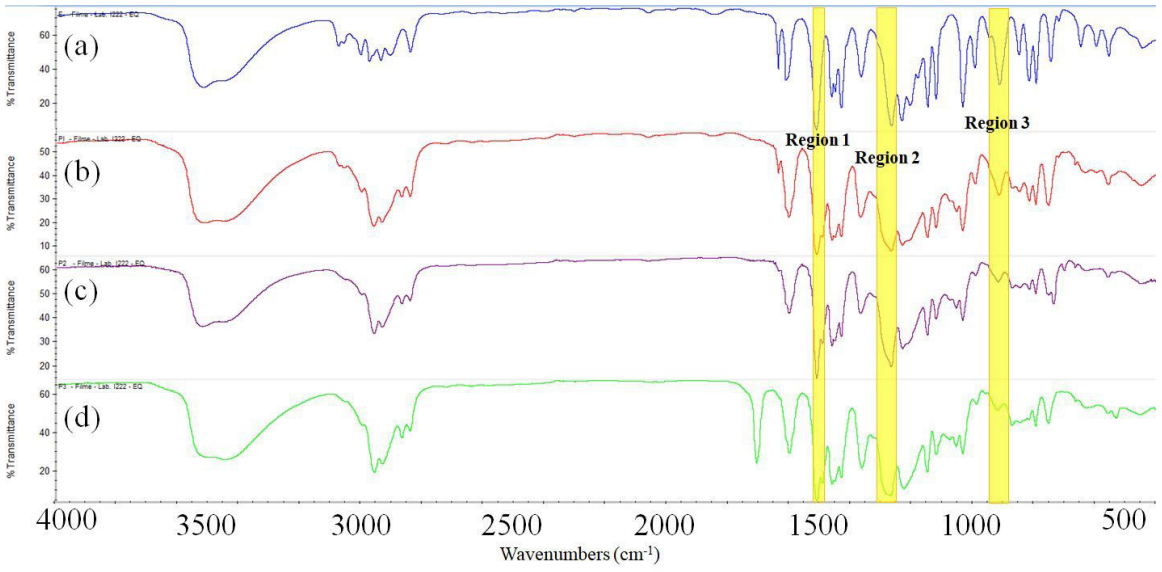

Figure 2. FTIR spectra: (a) eugenol, (b) P10, (c) P20, and (d) P30.

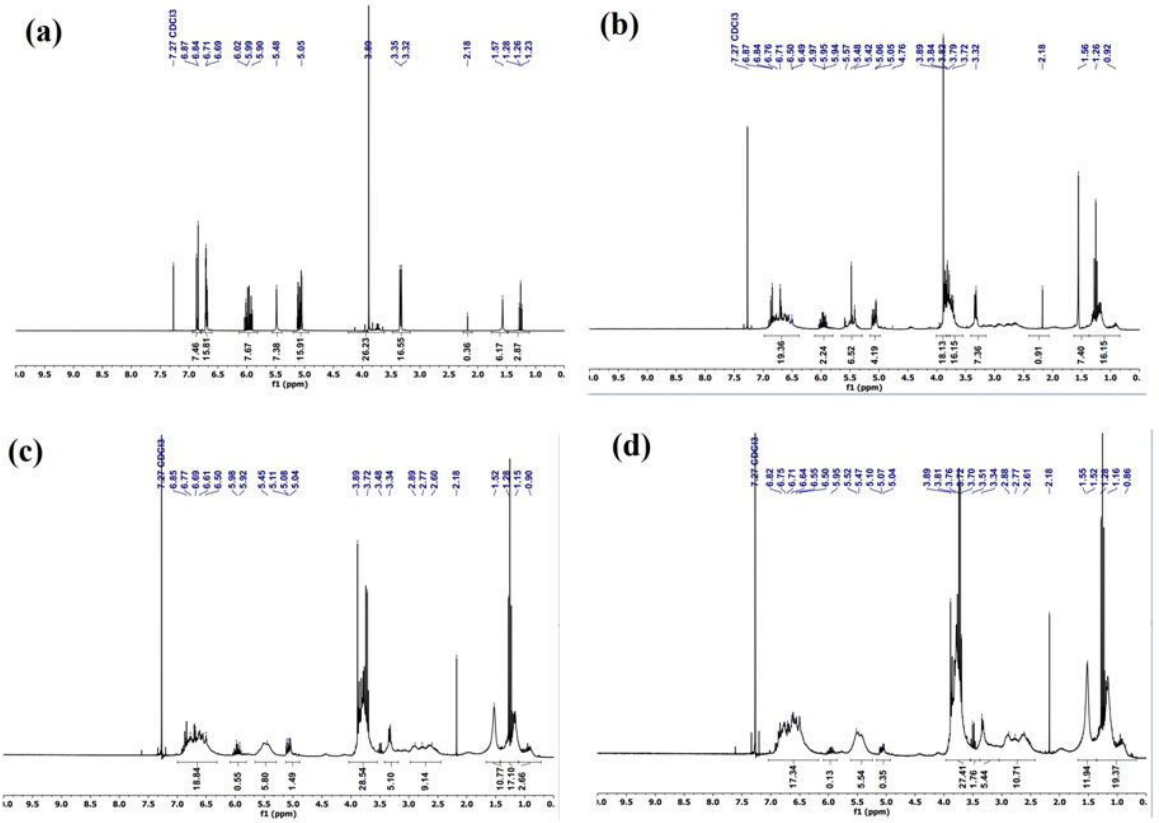

Figure 3. ^{1}H-NMR spectra of (a) eugenol, (b) P10, (c) P20, and (d) P30.

ratio ($R_{i/m}$), suggesting a greater degree of polymerization. The presence of vinylic hydrogen was evident in the form of chemical shifts at 5.04-5.11 and 5.90-6.02 ppm[45], which decline with a rise in $R_{i/m}$, thereby confirming polymerization. The reaction conversions can also be estimated by the ratio between the areas under the vinylic hydrogen signals for eugenol and the respective oligomer. The polymerization conversions were 72.3, 91.7 and 98.1% for P10, P20 and P30, respectively.

3.1.3. Thermogravimetric analysis (TGA/DTG)

The thermal analyses of the oligomers (P10, P20 and P30) are presented in Figure 4 (thermogravimetric analysis – TGA; derivative thermogravimetry - DTG). Water content is lower than 1.5%, evident at around 373 K. Residual mass increases with a rise in initiator concentration. P30 exhibits the highest residual mass, possibly due to its higher polymerization degree, leading to more thermally stable rearranged structures under the analysis conditions.

There are three main exothermic events, at 414-438, 521-533 and 629-637 K (T_{onset}). The first corresponds to evaporation of free eugenol, side chains and low molecular weight substances and the second suggests the degradation of encapsulated non-reacted eugenol[46,47]. The intensity of this event declines when the initiator/monomer ratio increases, due to the higher degree of polymerization. As such, P10 shows a more intense event in Figure 4b, and P30 a less significant event. This corroborates the reaction conversion,

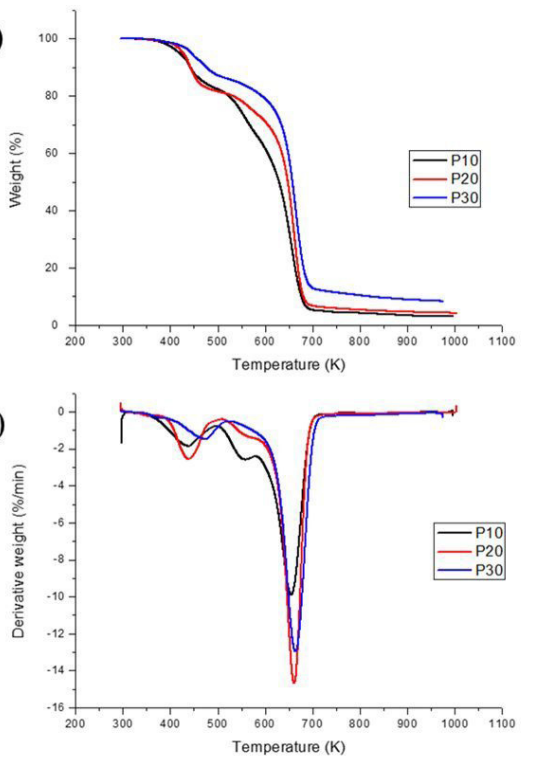

Figure 4. Thermal analyses of P10, P20 and P30: (a) TGA, and (b) DTG.

indicated by the decreasing amount of non-reacted eugenol, and confirms the FTIR and ^{1}H-NMR analyses.

The most intense event, observed at 629-637 K, is attributed to the degradation of the polymeric chain. The results indicate that polyeugenol is more thermally stable (629-637 K) than pure eugenol, which is reported to degrade between 320 and 470 K[46,47]. This greater thermal stability is of special interest because it enables polyeugenol to be used in corrosion inhibition applications at higher temperatures.

3.1.4. Size exclusion chromatography (SEC)

The size exclusion chromatography results are summarized in Table 1. In SEC, number-average molecular weight (M_n) and weight-average molecular weight (M_w) can be determined simultaneously. In addition, the M_w/M_n ratio is used to calculate the polydispersity index (PDI), an indicator of molecular weight distribution. M_n and M_w can be calculated using Equations 5 and 6[48]:

$$M_n = \frac{\Sigma(M_i N_i)}{\Sigma N_i} \quad (5)$$

$$M_w = \frac{\Sigma\left(M_i^2 N_i\right)}{\Sigma(M_i N_i)} \quad (6)$$

where N_i is the number of polymer molecules and M_i the molecular weight. According to Equation 5, M_n is the simple arithmetic mean, which is sensitive to the presence of low molecular weight compounds and M_w the weight-average molecular weight, sensitive to the presence of high molecular weight compounds[48,49].

M_w increases with a rise in the initiator/monomer ratio. However, the behavior of the polydispersity index (PDI) shows a maximum value of 1.89 for P20, suggesting a more heterogenic polymeric chain, followed by P30 and P10, respectively.

3.2. Weight loss measurements

Figures 5a and 5b show the corrosion rates and inhibition efficiencies for P10, P20 and P30 at 333 K. The significant decrease in the corrosion rate (CR) for the systems containing the oligomers confirms the inhibitory ability of the synthesized inhibitors.

The concentration effect was similar for all the oligomers. From 0.5 to 2.0% v/v, reductions of 17.00, 20.81 and 16.00% of CR were observed for P10, P20 and P30, respectively. However, an additional concentration increase (2.0 to 5.0% v/v) showed only a minor contribution to the decline in CRs, which were in the same order of magnitude considering the standard deviation. The coefficient of variation (CV) was calculated to assess reproducibility, with low CV values indicating greater experimental precision for a certain parameter. The CV was calculated using the CR values of the replica, with all the CVs below 15%, which is considered acceptable[50,51]. Thus, the optimum concentration for all oligomers is 2.0% v/v (Table 2).

The compound with the lowest polymerization degree, P10, exhibited the highest inhibition efficiency at all concentrations. P30 (highest polymerization degree) displayed intermediate efficiency in relation to P10 and P20, at 0.5% v/v. However, at higher concentrations, P30 and P20 exhibited similar inhibition efficiency (considering standard deviation). This can be attributed to the higher polymerization degree of these two oligomers, likely causing steric effects between the molecules in the bulk solution and hampering diffusion. These effects interfere in the adsorption to the substrate. Both of these oligomers exhibit similar effects at higher concentrations, when their

Table 1. Size exclusion chromatography results obtained for oligomers P10, P20 and P30: Mn, Mw, degree of polymerization and PDI.

Oligomer	Initiator (g)/ monomer (g)	M_n	M_w	Degree of polymerization	PDI
P10	0.10	416	743	4.5	1.78
P20	0.20	466	885	5.4	1.89
P30	0.30	504	930	5.7	1.84

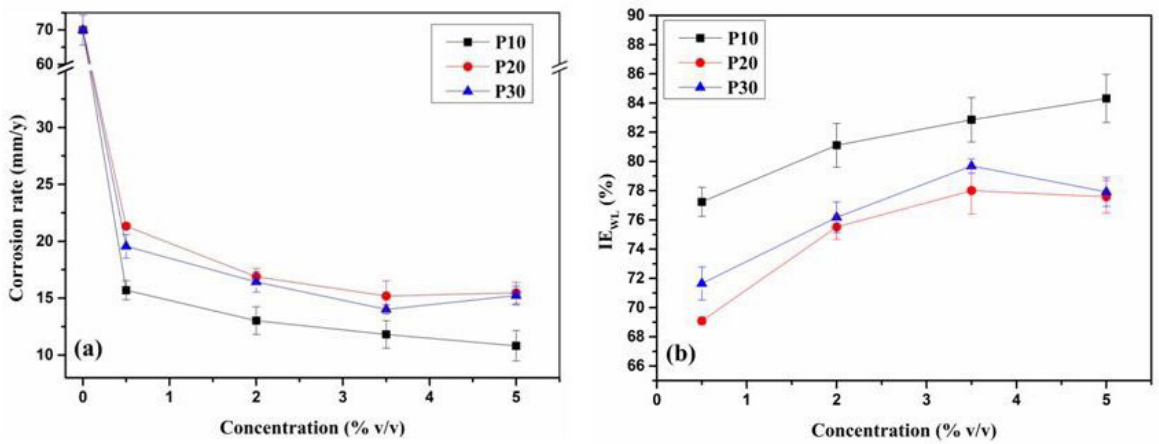

Figure 5. Effect of concentration on the corrosion rate (a) and inhibition efficiency (b) of P10, P20 and P30 in HCl 1M at 333 K.

Table 2. Weight loss data for P10, P20 and P30 in HCl 1M at 333 K.

Inhibitor	Concentration (%v/v)	Corrosion rate (mm/y)	Inhibition efficiency (%)
Blank	0.0	69.98±4.38	-
P10	0.5	15.70±0.84	77.24±0.99
	2.0	13.03±1.22	81.11±1.50
	3.5	11.82±1.20	82.86±1.52
	5.0	10.82±1.34	84.32±1.64
P20	0.5	21.33±0.24	69.08±0.25
	2.0	16.89±0.73	75.51±0.84
	3.5	15.18±1.34	78.00±1.59
	5.0	15.46±0.94	77.59±1.12
P30	0.5	19.56±1.04	71.65±1.13
	2.0	16.43±0.91	76.18±1.05
	3.5	14.01±0.40	79.69±0.49
	5.0	15.23±0.83	77.92±0.98

effects are magnified. In fact, Chamovska et al.[52] reported that polydispersity affects adsorption, and adsorption rates are much slower as polydispersity increases. Therefore, P10 performed better due to its lower polydispersion, associated with molecules that have a lower molecular size, since it showed the lowest M_W of all three oligomers assessed. These two factors contribute to a small more uniform and molecular structure (lower PDI), allowing easier adsorption onto the metallic substrate and promoting better surface coverage. Besides, this structure information about P10 indicates that it might have higher mobility, corroborating the lowest corrosion rate in weight loss measurements. This mobility is associated with lower number of aromatic rings in the polymeric structure, resulting in efficient and more uniform coverage of the metallic surface.

The aromatic structure of polyeugenol is subject to steric and stiffness effects even in the presence of a small number of repeating units. This is specially noticed when comparing P10 to P20/P30 in the weight loss measurements (Table 1).

Chaieb et al.[27] studied eugenol and acetyl-eugenol as corrosion inhibitor for steel in 1 M HCl, reporting weight loss efficiencies at 298 K, after 1 h immersion, of 57 and 64%, respectively. At 328 K, the efficiencies increase to 78 and 87%, respectively. Among the eugenol oligomers synthesized in this work, the best performance was obtained for P10, exhibiting 84% after 24 h immersion at 333 K. Comparing the results, it can be observed that P10 shows efficiencies between eugenol and acetyl-eugenol. However, it is important to mention that Chaieb et al.[27] results are at 1 h immersion, while this work reports results at 24 h immersion. Therefore, the steel coupon is in the presence of the acidic solution for longer time and P10 is able to maintain the protection. In this sense, comparing the published results in literature with the obtained oligomers, P10 exhibited better protection than eugenol. Also, the ability to inhibit corrosion for longer exposure time is highly desirable for industrial applications which highlights the importance of the polymerization strategy to enhance the monomer protection. Thus, the selective oligomerization of eugenol is a good strategy for the production of tailor made molecules with greater corrosion inhibition potential in relation to the eugenol molecule and its possible derivatives.

3.2.1. Effect of concentration

The adsorption isotherms (Langmuir, Temkin, Frumkin and El-Awady) were calculated according to Equations 7-10, respectively, where C is the oligomer concentration, K_{ads} the adsorption constant, g represents lateral interactions between the molecules and θ is surface coverage[53,54].

$$\frac{C}{\theta} = \frac{1}{K_{ads}} + C \quad \text{(Langmuir isotherm)} \tag{7}$$

$$\theta = \left(\frac{-2.303}{2a}\right)\log K + \left(\frac{-2.303}{2a}\right)\log C \quad \text{(Temkin isotherm)} \tag{8}$$

$$log_{10}\left(\frac{C}{\theta}\right) = \log_{10} k_{ads} + g\theta \quad \text{(Frumkin isotherm)} \tag{9}$$

$$\log\frac{\theta}{1-\theta} = \log K + y\log C \quad \text{(El Awady isotherm)} \tag{10}$$

The variation in standard Gibbs free energy for adsorption (ΔG^{0}_{ads}) was calculated using Equation 11, where R is the ideal gas constant (8.314 $J\cdot mol^{-1}\cdot K^{-1}$), T the temperature in K, and 55.5 the water content in $mol\cdot L^{-1}$.

$$K_{ads} = \frac{1}{C(solvent)} exp\left(\frac{\Delta G^{\circ}_{ads}}{RT}\right) \tag{11}$$

The parameters (Table 3) were calculated based on weight loss measurements. The Langmuir isotherm provided the best fit (Figure 6). According to this model, the adsorption of molecules can be represented by an inhibitor monolayer on the metallic surface, in which adsorption sites have equivalent energy level and electronic affinity, and the adjacent adsorbed molecules are supposedly free from steric effects or lateral interactions[55]. High K_{ads} values indicate better interaction between the molecules and substrate, and low K_{ads} values suggest weak interactions, enabling easy removal by solvent molecules[56,57]. Although P10 obtained the lowest CR, P30 exhibited the strongest adsorption, followed by P10. P30 has a greater degree of polymerization than P10, resulting in a non-continuous film on the substrate and leading to a higher CR. However, P30 has a higher M_w, indicating more

stable highly structured molecules with a stronger adsorption force, supporting its higher K_{ads}.

Negative ΔG^0_{ads} values demonstrate spontaneous adsorption, as observed in Table 2. For $|\Delta G_{ads}|$ less than 20 kJ·mol^{-1}, adsorption is defined as physisorption, > 40 kJ·mol^{-1} as chemisorption, and between $20 < |\Delta G_{ads}| < 40$ kJ·mol^{-1}, both physisorption and chemisorption[3,12,58]. Physical and chemical adsorption were observed for all the oligomers.

3.2.2. Effect of temperature

The Arrhenius equation (Equation 12) relates the CR to the apparent activation energy of dissolution in steel (E_a), where R is the universal constant of ideal gases (8.314 J/mol K), T the absolute temperature and A the pre-exponential factor.

$$\log CR = \frac{-E_a}{2.303RT} + \log A \quad (12)$$

The E_a values were obtained for each oligomer via linear adjustments of the data (Table 4 and Figure 7). All the quadratic regression coefficients (R^2) were above 0.98, indicating that the corrosion mechanism can be precisely explained by the Arrhenius kinetic model.

The E_a value in the absence and presence of corrosion inhibitors provides information on the inhibitory mechanism.

Table 3. Langmuir, Temkin, El-Awady and Frumkin coefficients of determination (R^2), slopes and K_{ads} for P10, P20 and P30 at 333 K.

Inhibitor	Langmuir				Temkin		El Awady		Frumkin	
	K_{ads} (L mg^{-1})	R^2	Slope	$-\Delta G_{ads}$ (kJ mol^{-1})	R^2	Slope	R^2	Slope	R^2	Slope
P10	11.2360	0.9998	1.1737	25.8193	0.9950	-13.8020	0.9880	0.1941	0.9974	17.146
P20	10.7991	0.9999	1.2667	25.7095	0.9531	-9.8443	0.9598	0.2057	0.9709	12.6750
P30	15.6986	0.9994	1.2615	26.7452	0.8685	-11.3630	0.8631	0.1724	0.9145	14.300

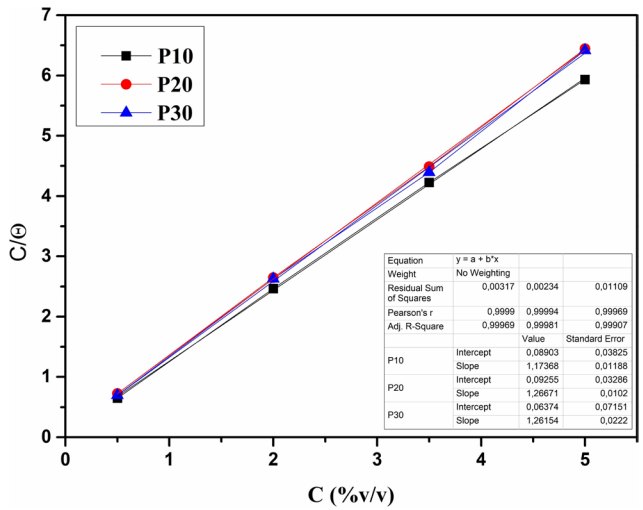

Figure 6. Langmuir adsorption isotherm for P10, P20 and P30 at 333 K.

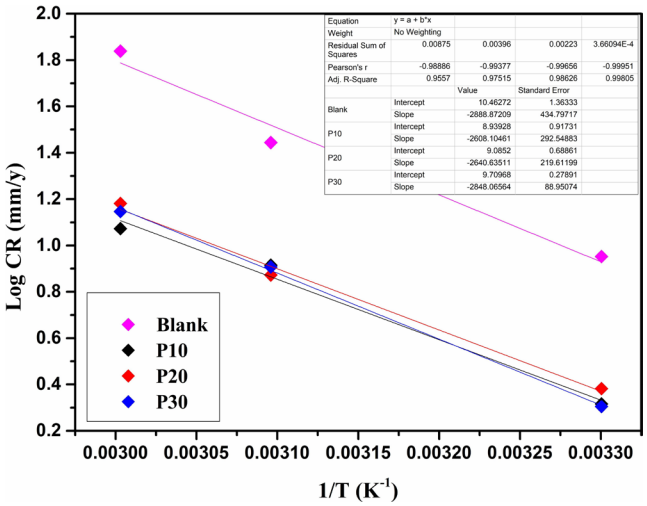

Figure 7. Arrhenius plots for API P110 carbon steel in 1 M HCl in the absence and presence of the inhibitors (3.5%v/v).

Previous studies[56,59-61] related chemical and physical adsorption to temperature effects. The E_a value obtained in the absence of inhibitors is a reference value for inhibited systems. When efficiency declines with a rise in temperature, the E_a value is higher for inhibited systems, indicating coulombic or physical adsorption, while chemical adsorption occurs when efficiency increases with temperature, and E_a is lower for the inhibited system. The E_a value of API P110 steel in 1 M HCl, without corrosion inhibitors, was 64.51 kJ/mol, corroborating previous studies[62-65].

Apparent activation energy values for the oligomers at 3.5% v/v were very similar and lower than the E_a value of the blank. Since these values are lower, but pretty close to the blank, the adsorption mechanism can be characterized as chemical and physical, as demonstrated by the isotherm model.

3.3. Electrochemical measurements

3.3.1. Open circuit potential (OCP) measurements

OCP was monitored in the presence and absence of the oligomers (P10, P20 and P30) (Figure 8). It should be noted that only 2.0% v/v was studied in the electrochemical tests, since the WL measurements indicated that this is the optimal concentration for all inhibitors. In general, the presence of a corrosion inhibitor shifted the E_{OCP} in the anodic direction, i.e. more noble potentials, suggesting surface protection against the acidic media[66-68]. The corrosion potential stabilized after 50 min for all the inhibitors, indicating the formation of a stable film over the surface. Overall, the highest E_{OCP} was recorded for P10 and may be related to its lower molecular size and major mobility, favoring film formation.

Table 4. E_a values for API P110 carbon steel in 1 M HCl for the inhibited and non-inhibited systems (3.5% (v/v)).

Test	E_a (kJ mol^{-1})	R^2
Blank	55.31	0.9888
P10	49.94	0.9937
P20	50.56	0.9965
P30	54.53	0.9995

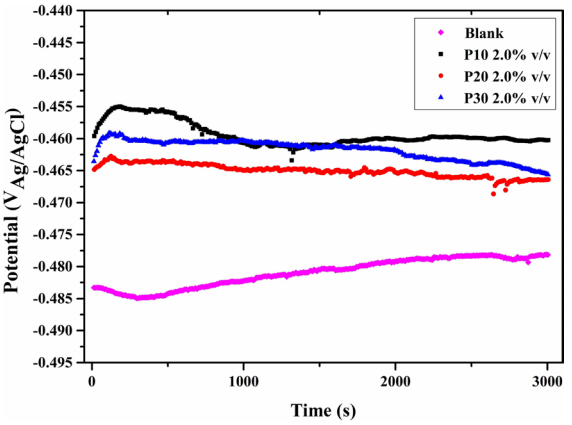

Figure 8. OCP for API P110 carbon steel coupons in the absence and presence of P10, P20 and P30 (2.0% v/v) at 298 K.

3.3.2. Linear polarization resistance (LPR) measurements

The relation between electrochemical potential and current density is shown in Figure 9. Linear polarization resistance is an efficient nondestructive method for determining the real-time corrosion rate because it scans a reduced range around the corrosion potential. The ±15 mV interval is within the limits for i_{corr} and E and allows subsequent measurements because it does not significantly or permanently interfere in corrosion[69].

Polarization resistance (R_p) is determined by the angular coefficient of the linear interpolation of data. All interpolations resulted in an R^2 of at least 0.9959, and the standard deviation percentage in relation to the arithmetic mean of replica R_p was below 14.27%, indicating good reproducibility[50,51]. Inhibitor

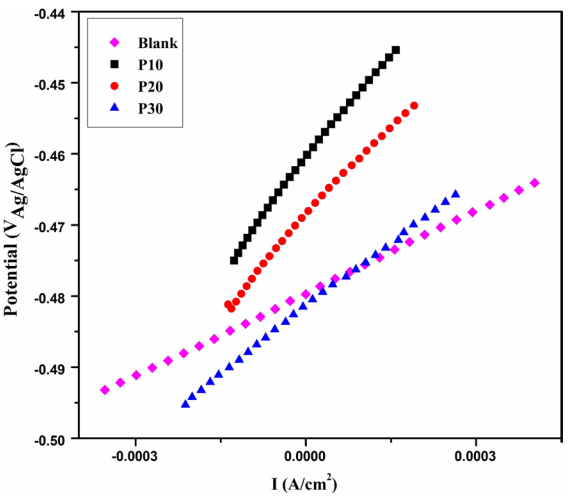

Figure 9. Linear polarization resistance curves for immersed API P110 carbon steel coupons in the absence and presence of P10, P20 and P30 (2.0% v/v), at 303 K.

Table 5. Electrochemical parameters for API P110 carbon steel in the absence and presence of P10, P20 and P30 (2.0% v/v) in 1 M HCl at 303 K.

Oligomer	LPR				PDP				
	Rp (Ω cm^{-2})	Standard deviation (%)	R^2	IE_{LPR} (%)	Ecorr (mV)	|βc| (mV/dec)	βa (mV/dec)	I_{corr} (μA/cm^2)	IE_{PDP} (%)
Blank	38.78	8.83	0.9999	-	504.30	48.5	20.28	42.52	-
P10	102.67	9.64	0.9971	62.23	458.46	25.67	21.62	10.98	74.18
P20	87.90	4.85	0.9960	55.88	464.92	37.34	15.21	13.48	68.30
P30	67.06	6.39	0.9967	42.18	468.85	33.20	14.48	13.79	67.57

efficiency (IE_{LPR}) was calculated using Equation 4. When compared to the blank, angular coefficients were higher for all the conditions assessed, demonstrating that the oligomers protected the metallic surface from corrosion.

The polarization resistance and inhibition efficiency values are summarized in Table 5. Oligomer P10 exhibited the highest R_p at all concentrations, followed by P20 and P30. Additionally, P10 achieved the best results in terms of weight loss and electrochemical testing, indicating that a lower degree of polymerization leads to better surface coverage. The greater size and rigidity of P30 (higher M_w) resulted in lower diffusion towards the metallic surface in the liquid phase at a lower temperature (298 K when compared to 333 K of the WL measurements). This explains that P20 is better able to approach the metallic surface at the low temperature and exposure time of the electrochemical tests when compared to P30[26]. Therefore, the mobility is associated with lower molecular volume of the polymeric structure, resulting in more efficient coverage of the metallic surface and higher inhibition efficiencies.

It is important to underscore that the lower inhibition efficiencies achieved in electrochemical tests when compared to weight loss measurements is related to the temperature of the tests. The hypothesis that can be generated to explain this observation is as follows: since electrochemical tests were performed at 303 K, the mobility (diffusion) of the macromolecules was insufficient to achieve complete surface coverage, while the weight loss measures at 333 K lead to a probable better performance at higher temperatures. This efficiency increase can be observed by the following weight loss efficiencies of P10 from 313 to 333 K at 2.0%v/v: 59.33% (313 K), 76.21% (323 K) and 81.11% (333 K).

3.3.3. Potentiodynamic polarization (PDP) measurements

Anodic and cathodic curves for the three oligomers (P10, P20 and P30) are depicted in Figure 10 and Table 5. Inhibition efficiency (IE_{PDP}) was calculated by Equation 3. In the present study, the Tafel extrapolation method was applied to obtain corrosion rates for activated-controlled processes. Accurate use of Tafel extrapolation requires that the interval considered be at least 50-100 mV from the corrosion potential and at least one of the branches should exhibit linearity on the semilogarithmic scale over a minimum of one decade of current density[70].

According to Figure 10, addition of the inhibitor affected the corrosion reactions for all three inhibiting solutions (P10, P20 and P30), more specifically the anodic branch, which is more linear in the presence of P20 and P30. It can be seen that the anodic and cathodic curves for the blank test are more polarized than in the presence of the inhibitors, this observation being more evident in the cathodic branch. As can be seen in Figure 8, the OCP curve of the blank shows a certain potential variation over the 50 min of immersion, which is associated with the formation of corrosion products on the metallic surface. Such a layer of corrosion products conferred some protection to the specimen, as observed by both anodic and cathodic current densities. However, when

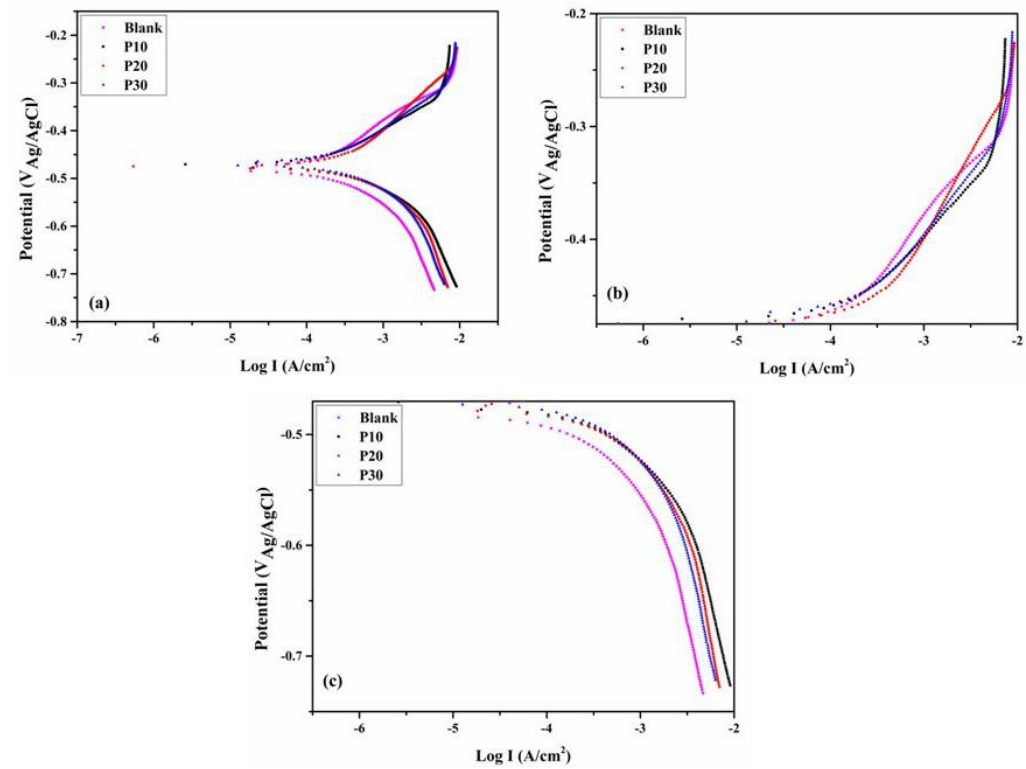

Figure 10. Potentiodynamic polarization curves for immersed API P110 carbon steel coupons in the absence and presence of P10, P20 and P30 at 303 K (a); anodic branches (b) and cathodic branches (c).

comparing such current densities with tests in the presence of inhibitors, it should be kept in mind that Table 2 shows that the protection provided by the inhibitors is undeniable, given that the corrosion rate of the blank is higher (69.98 mm/y), for example, than P10 5.0%v/v (10.82 mm/y). In this sense, the explanation for the anodic and cathodic current densities of the inhibitor tests being higher than the blank lies in the fact that the electrochemical test time was 50 minutes, less than the mass loss (24 h), not having been sufficient to form the proper coating on the metal surface, and not a blank-like oxide layer. Possibly, if the tests were performed at longer times, the protective layer of inhibitor would promote a continuous and more efficient covering of the surface, observing behavior closer to that verified in the loss of mass, with current displacements greater than the blank, not only in the OCP as well as polarization region.

P10 exhibited the lowest I_{corr} and, consequently, the greatest inhibition efficiency, which is consistent with LPR and weight loss measurements. A corrosion inhibitor is mixed if its presence shifts the open circuit potential to between -85 and +85 mV in relation to the blank[66-68]. Since the maximum shift between the corrosion potential of the blank and in the presence of the inhibitors was 45 mV, they can be classified as mixed-type. Moreover, the anodic and cathodic branches showed similar curves with and without the inhibitors, indicating that the corrosion mechanism remained unchanged[71-73]. In this sense, the oligomers are mixed type adsorption inhibitors, which limit the HCl access to the metal surface, so reducing the corrosion rate. The adsorption on both anodic and cathodic sites may occur through the aromatic rings, which are high electron density centers that interact with the metallic surface.

3.4. SEM-EDX

The carbon steel surfaces with and without the inhibitor were analyzed by scanning electron microscopy (SEM) and their compositions obtained by energy-dispersive X-ray spectroscopy (EDX). The surface morphologies are shown in Figure 11 and chemical composition in Table 6.

When compared to the API P110 coupon with P10 (Figure 11b.1), the inhibitor-free sample surface is rougher and non-uniform (Figure 11a.1), while the steel surface in Figure 11b.1) is considerably smoother and more uniform, demonstrating that the inhibitor film adsorbed onto the surface and protected the coupon from the corrosive process.

The presence of the inhibiting film was also evident in EDS analysis (Table 6). In order to understand the increase in the amount of oxygen and carbon on the metallic surface, associated with adsorption of the inhibitor molecules, the C/Fe and O/Fe ratios were calculated. The surface without the inhibitor (Figure 11a.2) consisted mainly of iron (90.55%-wt), representing carbon steel, with C/Fe and O/Fe ratios[23,26,74] of 7.74 and 2.69%, respectively. In inhibited systems these

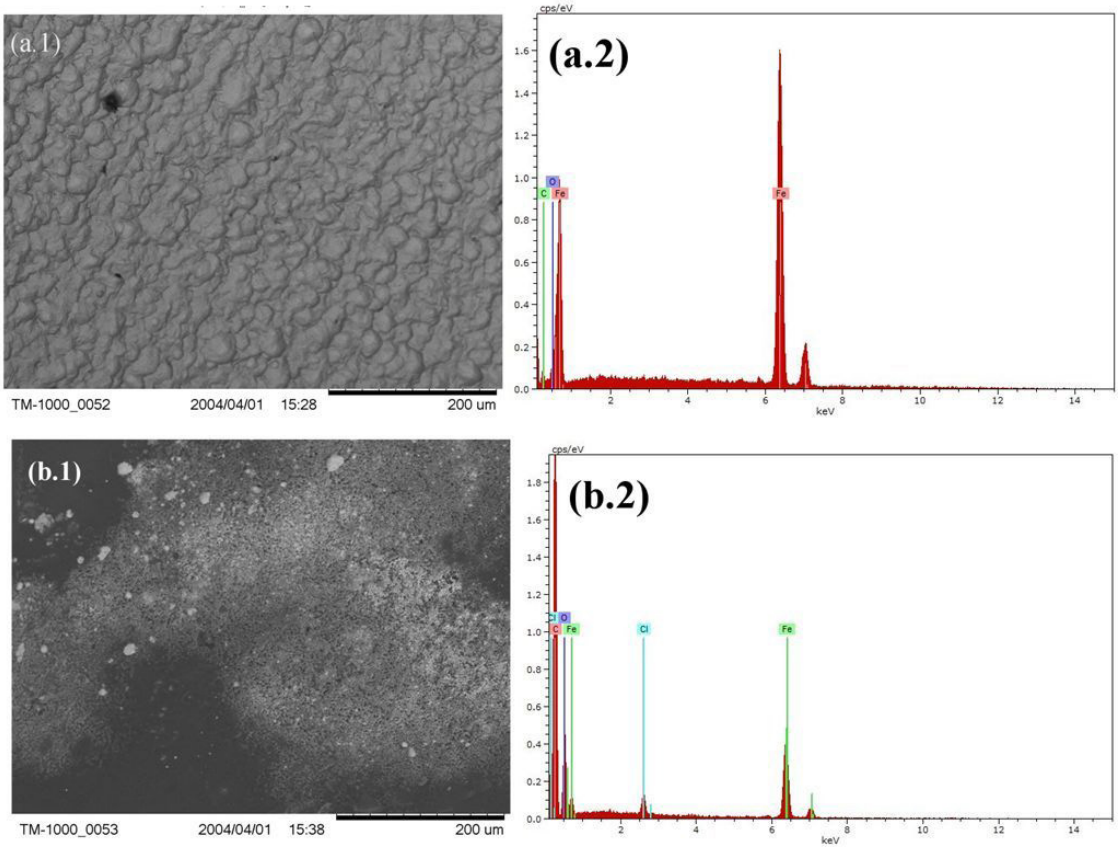

Figure 11. SEM and EDX of API P110 carbon steel after the 24-h immersion test in 1 M HCl at 333 K, without (a.1-a.2) and with 3.5% v/v of P10 (b.1-b.2).

Table 6. Element percentages according to SEM-EDX analysis of API P110 carbon steel in the absence and presence of P10 (3.5% v/v) at 333 K.

Test	Element	%Mass	C/Fe (%)	O/Fe (%)
Blank	Fe	90.55	7.74	2.69
	C	7.01		
	O	2.44		
P10	Fe	24.11	243.92	66.19
	C	58.81		
	O	15.96		
	Cl	1.12		

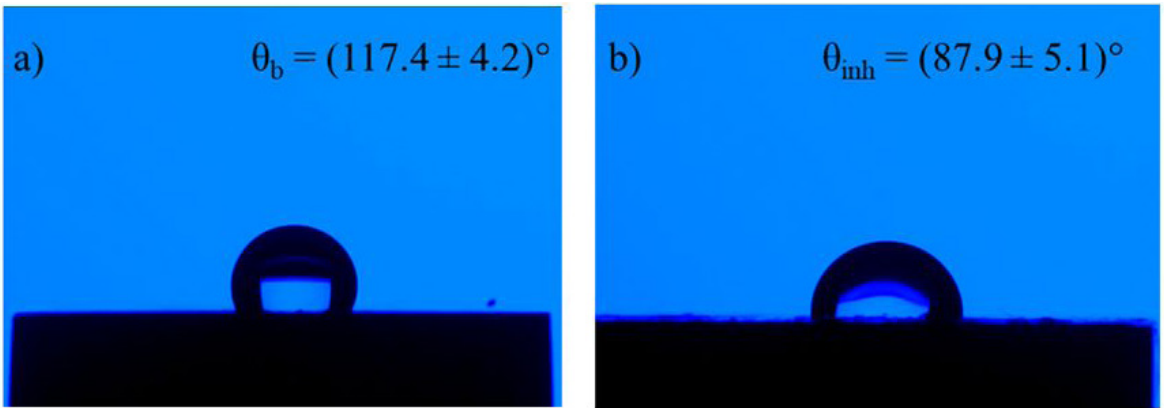

Figure 12. Contact angle images of API P110 carbon steel samples after 24 h of immersion in 1 M HCl at 333 K (a) without and (b) with the corrosion inhibitor (P10, 3.5% v/v).

values increased to 243.96 and 66.19% (Table 6), respectively, indicating adsorption of the corrosion inhibitor onto the metallic surface.

3.5. Contact angle

Figure 12 shows the contact angles of coupon surfaces with and without the inhibitor (P10, 3.5% v/v). After the 24-h immersion test, the contact angle of the uninhibited coupon was 117.4±4.2°, decreasing to 87.9±5.1° without it. An increase in the contact angle would be expected in the presence of an inhibiting film, characterizing greater hydrophobicity, as reported in the literature[75,76]. This reduction in the angle may be related to the adsorption of hydrophilic compounds, such as hydroxyl groups, in the most superficial film layer, favoring water bonding and decreasing hydrophobicity. As such, this technique is indicative of how the inhibiting structure adsorbs onto the metallic surface. The greater tendency observed in literature was not detected here, demonstrating the influence of the chemical nature of the inhibiting film adsorbed onto the metallic surface. Besides, another explanation based on the rugosity is related to the formation of air pockets in the micro-cracks present in the metallic surface more attacked by the acid solution in the absence of inhibitor, according to Cassie and Baxter model[77]. Thus, the non-inhibited system presents a greater presence of roughness and, consequently, a greater presence of cracks, which leads to a greater formation of air pockets and a greater apparent contact angle than the inhibited system.

4. Conclusion

This article studied the synthesis of a novel green corrosion inhibitor obtained from eugenol polymerization for API P110 carbon steel. In order to evaluate the influence of the initiator/monomer ratio on corrosion inhibition, three synthesized oligomers (0.10, 0.20 and 0.30 g-initiator/monomer – P10, P20 and P30) were characterized by FTIR, ^{1}H-NMR, TGA/DTG and SEC, which confirmed the polymerization reaction.

The electrochemical tests confirmed that the oligomers act as mixed inhibitors at an optimal concentration of 2.0% v/v, adsorbing on both anodic and cathodic sites. The difference in inhibition efficiency between P20 and P30 observed via LPR and PDP tests was explained based on SEC analysis, which indicated that P20 performed better than P30 due to structures with a lower molecular weight.

High-mobility oligomers, such as P10, exhibit the lowest corrosion rate in weight loss measurements. This mobility is associated with the less rigidity given by the aromatic ring in the oligomeric structure, resulting in efficient and more uniform coverage of the metallic surface. Although the polymerization degree of the oligomers is similar, the bulky trisubstituted aromatic structure provides significant steric and stiffness effects even in the presence of few repetitive units. The lower polymerization degree of P10 associated with its lower PDI are responsible for its better inhibition.

The surface characterization techniques confirmed the formation of an organic film on the steel surface, whereas the contact angles suggested the adsorption of hydroxyl groups oriented towards the bulk solution in the surface film.

In this respect, the inhibitors studied here are eco-friendly and have not been previously investigated in the literature, demonstrating its potential to compete with conventional inhibitors due to the high efficiencies obtained.

5. Acknowledgements

The authors thank the Laboratory of Instruments and Research of the Department of Inorganic Chemistry, Institute of Chemistry, Federal University of Rio de Janeiro (IQ/UFRJ) for the FTIR analyses, E. Miguez for ^{1}H-NMR analyses and J. Menezes for the SEM-EDX analysis. This study was funded by the Conselho Nacional de Desenvolvimento Científico e Tecnológico (CNPq) [grant number 142269/2017-4].

7. References

1. El-Raouf MA, Khamis EA, Kana MTHA, Negm NA. Electrochemical and quantum chemical evaluation of new bis(coumarins) derivatives as corrosion inhibitors for carbon steel corrosion in 0.5 M H_2SO_4. J Mol Liq. 2018;255:341-53.
2. Heakal FET, Elkholy AE. Gemini surfactants as corrosion inhibitors for carbon steel. J Mol Liq. 2017;230:395-407.
3. Hu Z, Meng Y, Ma X, Zhu H, Li J, Li C, et al. Experimental and theoretical studies of benzothiazole derivatives as corrosion inhibitors for carbon steel in 1 M HCl. Corros Sci. 2016;112:563-75.
4. Zhang Z, Tian N, Zhang L, Wu L. Inhibition of the corrosion of carbon steel in HCl solution by methionine and its derivatives. Corros Sci. 2015;98:438-49.
5. Finšgar M, Jackson J. Application of corrosion inhibitors for steels in acidic media for the oil and gas industry: a review. Corros Sci. 2014;86:17-41.
6. Verma C, Haque J, Quraishi MA, Ebenso EE. Aqueous phase environmental friendly organic corrosion inhibitors derived from one step multicomponent reactions: a review. J Mol Liq. 2019;275:18-40.
7. Cherrak K, Belghiti ME, Berrissoul A, El Massaoudi M, El Faydy M, Taleb M, et al. Pyrazole carbohydrazide as corrosion inhibitor for mild steel in HCl medium: experimental and theoretical investigations. Surf Interfaces. 2020;20:100578.
8. Obot IB, Obi-Egbedi NO. Theoretical study of benzimidazole and its derivatives and their potential activity as corrosion inhibitors. Corros Sci. 2010;52:657-60.
9. Dehghani A, Bahlakeh G, Ramezanzadeh B, Ramezanzadeh M. Detailed macro-/micro-scale exploration of the excellent active corrosion inhibition of a novel environmentally friendly green inhibitor for carbon steel in acidic environments. J Taiwan Inst Chem Eng. 2019;100:239-61.
10. Mainier FB, Silva RRCM. As formulações inibidoras de corrosão e o meio ambiente. Engevista. 2004;6:106-12.
11. Keramatinia M, Ramezanzadeh B, Mahdavian M. Green production of bioactive components from herbal origins through one-pot oxidation/polymerization reactions and application as a corrosion inhibitor for mild steel in HCl solution. J Taiwan Inst Chem Eng. 2019;105:134-49.
12. Dehghani A, Bahlakeh G, Ramezanzadeh B. Green *Eucalyptus* leaf extract: a potent source of bio-active corrosion inhibitors for mild steel. Bioelectrochemistry. 2019;130:107339.
13. Wang Q, Tan B, Bao H, Xie Y, Mou Y, Li P, et al. Evaluation of *Ficus tikoua* leaves extract as an eco-friendly corrosion inhibitor for carbon steel in HCl media. Bioelectrochemistry. 2019;128:49-55.
14. Alibakhshi E, Ramezanzadeh M, Bahlakeh G, Ramezanzadeh B, Mahdavian M, Motamedi M. *Glycyrrhiza glabra* leaves extract as a green corrosion inhibitor for mild steel in 1 M hydrochloric acid solution: experimental, molecular dynamics, Monte Carlo and quantum mechanics study. J Mol Liq. 2018;255:185-98.
15. Ramezanzadeh M, Bahlakeh G, Sanaei Z, Ramezanzadeh B. Studying the *Urtica dioica* leaves extract inhibition effect on the mild steel corrosion in 1 M HCl solution: complementary experimental, ab initio quantum mechanics, Monte Carlo and molecular dynamics studies. J Mol Liq. 2018;272:120-36.
16. El-Etre AY, Ali AI. A novel green inhibitor for C-steel corrosion in 2.0 mol·L^{-1} hydrochloric acid solution. Chin J Chem Eng. 2017;25:373-80.
17. Bahlakeh G, Ramezanzadeh B, Dehghani A, Ramezanzadeh M. Novel cost-effective and high-performance green inhibitor based on aqueous *Peganum harmala* seed extract for mild steel corrosion in HCl solution: detailed experimental and electronic/atomic level computational explorations. J Mol Liq. 2019;283:174-95.
18. Raghavendra N, Bhat JI. Red arecanut seed extract as a sustainable corrosion inhibitor for aluminum submerged in acidic corrodent: an experimental approach towards zero environmental impact. Period Polytech Chem Eng. 2018;62:351-8.
19. Hassannejad H, Nouri A. Sunflower seed hull extract as a novel green corrosion inhibitor for mild steel in HCl solution. J Mol Liq. 2018;254:377-82.
20. Pal S, Lgaz H, Tiwari P, Chung IM, Ji G, Prakash R. Experimental and theoretical investigation of aqueous and methanolic extracts of *Prunus dulcis* peels as green corrosion inhibitors of mild steel in aggressive chloride media. J Mol Liq. 2019;276:347-61.
21. Singh MR, Gupta P, Gupta K. The litchi (*Litchi Chinensis*) peels extract as a potential green inhibitor in prevention of corrosion of mild steel in 0.5 M H_2SO_4 solution. Arab J Chem. 2019;12(7):1035-41.
22. Mourya P, Banerjee S, Singh MM. Corrosion inhibition of mild steel in acidic solution by *Tagetes erecta* (Marigold flower) extract as a green inhibitor. Corros Sci. 2014;85:352-63.
23. Furtado LB, Rocha JC, Gomes JACP, Nascimento RC, Seidl PR, Guimarães MJOC, et al. Storage time evaluation of a residue from wine industry as a microencapsulated corrosion inhibitor for 1 M HCl. Mater Chem Phys. 2020;256:123739.
24. Singh MR, Gupta P, Gupta K. The litchi (*Litchi Chinensis*) peels extract as a potential green inhibitor in prevention of corrosion of mild steel in 0.5 M H_2SO_4 solution. Arab J Chem. 2019;12:1035-41.
25. Barreto LS, Tokumoto MS, Guedes IC, Melo HG, Amado FDR, Capelossi VR. Evaluation of the anticorrosion performance of peel garlic extract as corrosion inhibitor for ASTM 1020 carbon steel in acidic solution. Materia. 2017;22:e11852.
26. Furtado LB, Nascimento RC, Seidl PR, Guimarães MJOC, Costa LM, Rocha JR, et al. Eco-friendly corrosion inhibitors based on Cashew nut shell liquid (CNSL) for acidizing fluids. J Mol Liq. 2019;284:393-404.
27. Chaieb E, Bouyanzer A, Hammouti B, Benkaddour M. Inhibition of the corrosion of steel in 1 M HCl by eugenol derivatives. Appl Surf Sci. 2005;246:199-206.
28. Bhuiyan MNI. Constituents of the essential oil from leaves and buds of clove (*Syzigium caryophyllatum* (L.) Alston). Afr J Pharm Pharmacol. 2012;6:1260-3.
29. Singh G, Maurya S, De Lampasona MP, Catalan CAN. A comparison of chemical, antioxidant and antimicrobial studies of cinnamon leaf and bark volatile oils, oleoresins and their constituents. Food Chem Toxicol. 2007;45:1650-61.
30. Navikaite-Snipaitiene V, Ivanauskas L, Jakstas V, Rüegg N, Rutkaite R, Wolfram E, et al. Development of antioxidant food packaging materials containing eugenol for extending display life of fresh beef. Meat Sci. 2018;145:9-15.
31. Burt S. Essential oils: their antibacterial properties and potential applications in foods: a review. Int J Food Microbiol. 2004;94:223-53.

32. Ching-Hsiung L, Lin SH, Chi-Chen L, Yi-Chen L, Chao-Jung C, Ching-Liang C, et al. Inhibitory effect of clove methanolic extract and eugenol on dendritic cell functions. J Funct Foods. 2016;27:439-47.
33. Djunaidi MC, Siswanta D, Ulbricht M, Jumina J. Synthesis of Fe ionic-imprinted polyeugenol using polyethylene glycol diglycidilether as cross-linking agent for sorption of Fe(III). J Chem. 2015;15:305-14.
34. Fajrin A, Marliana S, Handayani DS. Synthesis of eugenol–lauryl methacrylate copolymers via cationic polymerization. IOP Conf Series Mater Sci Eng. 2018;349:012003.
35. Kiswandono AA, Siswanta D, Aprilita NH, Santosa SJ. Transport of phenol through inclusion polymer membrane (PIM) using copoly (eugenol-DVB) as membrane carriers. Indones J Chem. 2012;12:105-12.
36. Ciszewski A, Milczarek G. Polyeugenol-modified platinum electrode for selective detection of dopamine in the presence of ascorbic Acid. Anal Chem. 1999;71:1055-61.
37. Paul DW, Prajapati I, Reed ML. Electropolymerized eugenol: evaluation as a protective film for oxygen sensing. Sens Actuators B Chem. 2013;183:129-35.
38. ASTM: American Society for Testing and Materials. G31: standard practice for laboratory immersion corrosion testing of metals, 1972. West Conshohocken: ASTM; 2004.
39. Bentrah H, Rahali Y, Chala A. Gum Arabic as an eco-friendly inhibitor for API 5L X42 pipeline steel in HCl medium. Corros Sci. 2014;82:426-31.
40. Da Rocha JC, Gomes JACP, D'elia E. Corrosion inhibition of carbon steel in hydrochloric acid solution by fruit peel aqueous extracts. Corros Sci. 2010;52:2341-8.
41. Edelmann A, Lendl B. Toward the optical tongue: flow-through sensing of tannin-protein interactions based on FTIR spectroscopy. J Am Chem Soc. 2002;124:14741-7.
42. Oliveira MCC, Carvalho MG, Ferreira DT, Braz-Filho R. Flavonóides das flores de *Stiffitia chrysantha* Mikan. Quim Nova. 1999;22:182-4.
43. Fernández K, Agosin E. Quantitative analysis of red wine tannins using Fourier-transform mid-infrared spectrometry. J Agric Food Chem. 2007;55:7294-300.
44. Coates J. Interpretation of infrared spectra, a practical approach. In: Meyers RA, editor. Encyclopedia of analytical chemistry. Chichester: Wiley; 2006.
45. Pavia DL, Lampman GM, Kriz GS. Infrared spectroscopy: a guide for students of organic chemistry. Philadelphia: Saunder College Publishing; 1996.
46. Shao Y, Wu C, Wu T, Li Y, Chen S, Yuan C, et al. Eugenol-chitosan nanoemulsions by ultrasound-mediated emulsification: Formulation, characterization and antimicrobial activity. Carbohydr Polym. 2018;193:144-52.
47. Piletti R, Bugiereck AM, Pereira AT, Gussati E, Dal Magro J, Mello JMM, et al. Microencapsulation of eugenol molecules by β-cyclodextrine as a thermal protection method of antibacterial action. Mater Sci Eng. 2017;75:259-71.
48. Narain R. Polymer science and nanotechnology: fundamentals and applications. San Diego: Elsevier; 2020.
49. Rogošić M, Mencer HJ, Gomzi Z. Polydispersity index and molecular weight distributions of polymers. Eur Polym J. 1996;32:1337-44.
50. Faria DE Fo, Dias AN, Veloso ALC, Bueno CFD, Couto FAP, Matos JB Jr,, et al. Classification of coefficients of variation in experiments with commercial layers. Rev Bras Cienc Avic. 2010;12:255-7.
51. Lecler A, Savatovsky J, Balvay D, Zmuda M, Jean-Claude S, Galatoire O, et al. Repeatability of apparent diffusion coefficient and intravoxel incoherent motion parameters at 3.0 Tesla in orbital lesions. Eur Radiol. 2017;27:5094-103.
52. Chamovska D, Cvetkovska M, Grchev T. Corrosion inhibition of iron in hydrochloric acid by polyacrylamide. J Serb Chem Soc. 2007;72:687-98.
53. Santos EC, Cordeiro R, Santos M, Rodrigues PRP, Singh A, D'Elia E. Barley agro-industrial residues as corrosion inhibitor for mild steel in 1mol L^{-1} HCl solution. Mater Res. 2019;22:e20180511.
54. Ahamed KR, Farzana BA, Diraviam SJ, Dorothy R, Rajendran S, Al-Hashem A. Mild steel corrosion inhibition by the aqueous extract of commelina benghalensis leaves. Port Electrochem Acta. 2019;37:51-70.
55. Saha SK, Banerjee P. Introduction of newly synthesized Schiff base molecules as efficient corrosion inhibitors for mild steel in 1 M HCl medium: an experimental, density functional theory and molecular dynamics simulation study. Mater Chem Front. 2018;2:1674-91.
56. Gowraraju ND, Jagadeesan S, Ayyasamy K, Olasunkanmi L, Ebenso EE, Subramanian C. Adsorption characteristics of Iota-carrageenan and Inulin biopolymers as potential corrosion inhibitors at mild steel/sulphuric acid interface. J Mol Liq. 2017;232:9-19.
57. Khadom AA, Abd AN, Ahmed NA. *Xanthium strumarium* leaves extracts as a friendly corrosion inhibitor of low carbon steel in hydrochloric acid: kinetics and mathematical studies. S Afr J Chem Eng. 2018;25:13-21.
58. Musa AY, Kadhum AAH, Mohamad AB, Takriff MS. Molecular dynamics and quantum chemical calculation studies on 4, 4-dimethyl-3-thiosemicarbazide as corrosion inhibitor in 2.5 M H_2SO_4. Mater Chem Phys. 2011;129:660-5.
59. Oguzie EE. Evaluation of the inhibitive effect of some plant extracts on the acid corrosion of mild steel. Corros Sci. 2008;50:2993-8.
60. Behpour M, Ghoreishi SM, Gandomi-Niasar A, Soltani N, Salavati-Niasari M. The inhibition of mild steel corrosion in hydrochloric acid media by two Schiff base compounds. J Mater Sci. 2009;44:2444-53.
61. Nasser AJA, Sathiq MA. Comparative study of N-[(4-methoxyphenyl) (morpholin-4-yl)methyl]acetamide (MMPA) and N-[morpholin-4-yl(phenyl)methyl]acetamide (MPA) as corrosion inhibitors for mild steel in sulfuric acid solution. Arab J Chem. 2017;10:S261-73.
62. Aoun SB. On the corrosion inhibition of carbon steel in 1 M HCl with a pyridinium-ionic liquid: chemical, thermodynamic, kinetic and electrochemical studies. RSC Advances. 2017;7:36688-96.
63. Benabdellah M, Tounsi A, Khaled KF, Hammouti B. Thermodynamic, chemical and electrochemical investigations of 2-mercapto benzimidazole as corrosion inhibitor for mild steel in hydrochloric acid solutions. Arab J Chem. 2011;4:17-24.
64. Singh AK. Inhibition of mild steel corrosion in hydrochloric acid solution by 3-(4-((Z)-Indolin-3-ylideneamino)phenylimino) indolin-2-one. Ind Eng Chem Res. 2012;51:3215-23.
65. Hameed RSA. Ranitidine drugs as non-toxic corrosion inhibitors for mild steel in hydrochloric acid medium. Port Electrochim Acta. 2011;29:273-85.
66. Shaban SM, Aiad I, El-Sukkary MM, Soliman EA, El-Awady MY. Evaluation of some cationic surfactants based on dimethylaminopropylamine as corrosion inhibitors. J Ind Eng Chem. 2015;21:1029-38.
67. Murulana LC, Kabanda MM, Ebenso EE. Investigation of the adsorption characteristics of some selected sulphonamide derivatives as corrosion inhibitors at mild steel/hydrochloric acid interface: Experimental, quantum chemical and QSAR studies. J Mol Liq. 2016;215:763-79.
68. Lgaz H, Bhat S, Salghi R, Jodeh S, Hammouti B. Effect of clozapine on inhibition of mild steel corrosion in 1.0 M HCl medium. J Mol Liq. 2017;225:271-80.

69. Umoren SA. Polypropylene glycol: a novel corrosion inhibitor for × 60 pipeline steel in 15% HCl solution. J Mol Liq. 2016;219:946-58.
70. Badea GE, Caraban A, Dzitac S, Cret P, Setel A. Polarisation measurements used for corrosion rates determination. J Sustain Energy. 2010;1:1-4.
71. Zhang W, Yan-Chao W, Hui-Jing L. *Apostichopus japonicus* polysaccharide as efficient sustainable inhibitor for mild steel against hydrochloric acid corrosion. J Mol Liq. 2021;321:114923.
72. Zhang K, Yang W, Yin X, Chen Y, Liu Y, Le J, et al. Amino acids modified konjac glucomannan as green corrosion inhibitors for mild steel in HCl solution. Carbohydr Polym. 2018;181:191-9.
73. Fathima H, Pais M, Rao P. Anticorrosion performance of biopolymer pectin on 6061 aluminium alloy: electrochemical, spectral and theoretical approach. J Mol Struct. 2021;1243:130775.
74. Furtado LB, Nascimento RC, Guimarães MJOC, Henrique FJFS, Rocha JC, Seidl PR, et al. Cleaner corrosion inhibitors using *Peumus boldus* Molina formulations in oil well acidizing fluids: gravimetric, electrochemical and DFT studies. Sustain Chem Pharm. 2021;19:100353.
75. Atta AM, El-Mahdy GA, Al-Lohedan HA, Ezzat ARO. A new green ionic liquid-based corrosion inhibitor for steel in acidic environments. Mol. 2015;20:11131-53.
76. Reddy CM, Sanketi BD, Kumar SN. Corrosion inhibition of mild steel by Capsicum annuum fruit paste. Perspect Sci. 2016;8:603-5.
77. Cassie ABD, Baxter S. Wettability of porous surfaces. Trans Faraday Soc. 1944;40:546-51.